SILICON MONOLITHIC ACOUSTO-OPTIC MODULATOR

Suresh Sridaran and Sunil A. Bhave
Cornell University, Ithaca, NY, USA

ABSTRACT

This paper reports on the co-fabrication of RF MEMS radial contour mode resonators and photonic whispering gallery mode disk resonators on the same SOI substrate. By mechanically coupling the MEMS and photonic resonators, we have demonstrated a silicon acousto-optic modulator (AOM) which can modulate a 1550 nm laser at 288 MHz. An output RF power of -83.7 dBm is observed corresponding to a modulation of ±415 nW around a biased optical output of 3.98 µW. The AOM has a footprint of 50 µm × 30 µm and bandwidth of 24.2 kHz in vacuum due to a high mechanical quality factor (*Q*) of 11,890.

INTRODUCTION

Commercial off-the-shelf acousto-optic modulators work by launching a traveling acoustic wave with an inter-digitated transducer (IDT) into an acousto-optically active medium thereby creating a modulated refractive index in the medium [1]. Incident light is diffracted and frequency shifted from this index modulated region and can be processed depending on output direction. To shrink the acousto-optic modulator to chip-scale, structures to convert acoustic phase modulation into intensity modulation like the Mach-Zehnder interferometer [2] or photonic microcavities [3], [4] have been demonstrated. In this paper, we propose a scheme of modulation using MEMS disk resonators for exciting mechanical motion and to use the mechanical motion to modify the intensity transmission characteristics of a photonic disk resonator.

As significant mechanical motion in the disk is only excited when the electrical drive is at the resonant frequency, our modulator is narrowband. A particular application for the AOM is in the monolithic integration of opto-electronic oscillators into silicon. Opto-electronic Oscillators (OEOs) demonstrated by OEWaves and Luxtera [5], [6] have superior phase-noise performance compared to traditional quartz and acoustic-MEMS approaches in the 1-30 GHz range. Unlike crystal oscillators whose phase-noise performance is limited by the $f \cdot Q$ product of the resonators, the phase-noise of the OEOs is only dependent on the laser source and the optical delay element. However, these OEOs are hand-assembled using discrete components including a surface-acoustic wave (SAW) filter for frequency selection followed by a Mach-Zehnder modulator (MZM) for up-conversion. The signal chain consists of electrical

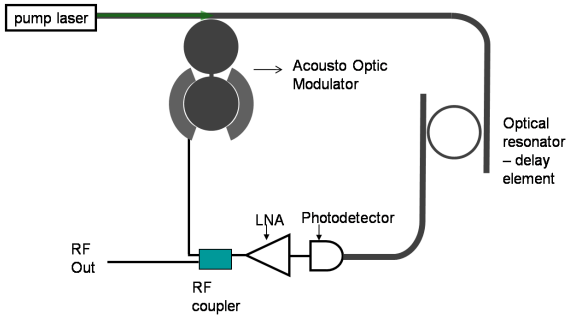

Figure 1. *Schematic of an opto-electronic oscillator with an acousto-optic modulator for selecting and up-converting the RF signal to optical frequency, photonic disk resonator as a high optical-Q, long time-delay element and germanium photo-detector [7] for down-conversion. All components can be monolithically fabricated in SOI, except the laser which can be surface-mount.*

→ acoustic-filter → electrical → impedance-match → electrical → optical. The silicon acousto-optic modulator monolithically integrates the signal processing into one device by elegantly converting the signal from electrical → acoustic-filter → optical (figure 1) with minimal inefficiency, < 100µm^2 foot-print and zero DC power consumption.

PRINCIPLE OF OPERATION

The schematic of an AOM consisting of two disk resonators coupled to each other by a mechanical beam is shown in figure 2. The resonator with electrodes acts as the electrical to mechanical transducer. By coupling vibrations to the photonic resonator through the coupling beam, the changing radius causes the optical resonant wavelength to shift back and forth. For a fixed input laser wavelength, the shifting of the optical resonance curve leads to intensity modulation at the output.

Photonic Resonator

The optical resonator in the AOM is a whispering gallery disk resonator. The light from the waveguide is dropped at the resonator when the wavelength corresponds to the resonance wavelength. This resonance occurs when the phase added in one roundtrip of the light around the disk is an integral multiple of 2π and can be represented by Eqn. 1 [8]

$$m \cdot \lambda_0 = 2\pi \cdot R \cdot n_{eff} \quad (1)$$

where m is an integer, λ_0 is free space wavelength at resonance, R is the radius of the disk and n_{eff} is the

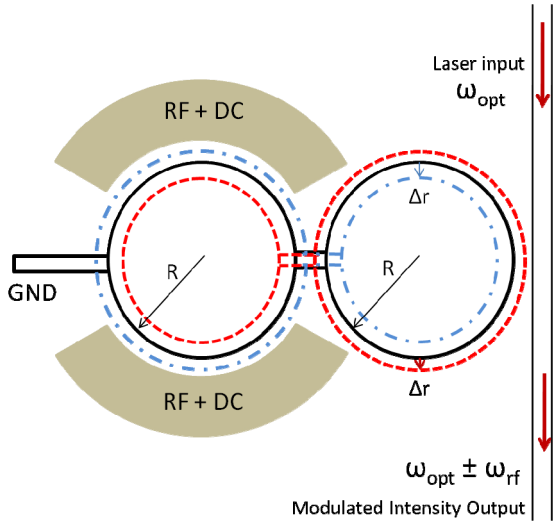

Figure 2. *The mechanical resonator (left) is excited with electrostatics which in turn transfers the vibrations to the photonic resonator (right) through the coupling beam. These vibrations of the photonic resonator change its circumference (dashes and dash-dots) and optical resonant frequency which in turn amplitude modulates the light through the waveguide.*

effective index of the mode at the radius of the disk obtained by solving the Maxwell's equations with appropriate boundary conditions. The transmission spectrum dip observed at the output of the waveguide is a Lorentzian centered at the resonant wavelength λ_0 as shown in figure 3. The optical quality factor ($Q_{optical}$) at critical coupling is related to full-width at half maximum (FWHM) by $Q_{optical} = \frac{\lambda_0}{FWHM}$. The depth of the dip is governed by the rate of energy decay of the resonator by absorption and scattering and the rate of energy coupling from the waveguide into the resonator [8].

The silicon AOM is a photonic resonator based modulator similar to electro-optic modulators that have been demonstrated [9]. In electro-optic modulators, the effective index is changed by charge injection to obtain a resonance wavelength shift. In an AOM, the radial vibrations change the radius by a small displacement Δr. This in turn changes the resonance wavelength to

$$m \cdot (\lambda_0 + \Delta\lambda) = 2\pi \cdot (R + \Delta R) \cdot n_{eff} \qquad (2)$$

which simplifies to

$$\frac{\Delta\lambda}{\lambda_0} = \frac{\Delta R}{R} \qquad (3)$$

The expected shift in the resonance wavelength for displacements of 0.5 nm for a 10μm disk with resonance at 1581.76 nm is approximately 80 pm and is shown in figure 3. It is observed that if the laser input is initially biased at the 3dB point of the transmission spectrum, then there is a modulation of the intensity at the output.

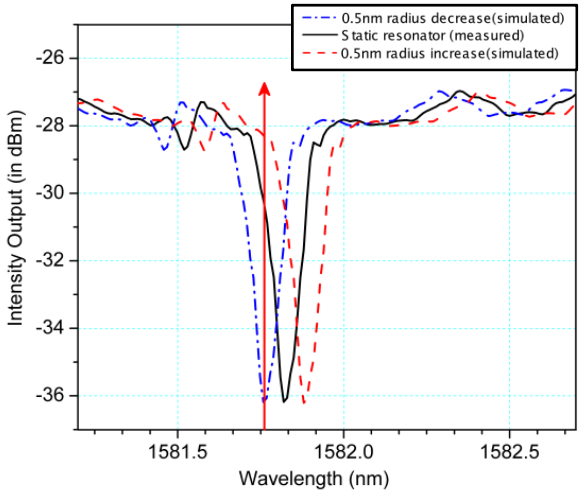

Figure 3. *Measured spectrum of a static photonic resonator with optical Q = 12,000. The laser (red arrow) is tuned half-way along the slope of the Lorentzian. A 0.5nm increase in radius is expected to cause a "red shift" turning off the resonator, whereas a 0.5nm decrease in radius would cause a "blue shift" and achieve critical coupling.*

Mechanical Resonator

The radial contour mode resonator is excited by using an air gap capacitive electrostatic transduction. The frequency of operation of the disk is obtained by solving [10]

$$\frac{\delta J_0(\delta)}{J_1(\delta)} = 1 - \sigma \qquad (4)$$

where $\delta = \omega_0 R\sqrt{\frac{\rho(1-\sigma^2)}{E}}$ where ω_0 is the angular resonant frequency, R is the radius of disk and ρ, E, σ are the density, Young's modulus and Poisson's ratio of silicon respectively and J_0 and J_1 are Bessel functions of the first kind.

We chose to employ separate disks for mechanical and photonic resonators to prevent the distortion and attenuation of the optical mode traveling in the photonic resonator from the free-electron charges on the MEMS resonator and the actuation electrodes. Further isolation is achieved by selectively implanting only the MEMS resonator while keeping the photonic resonator and waveguide region undoped.

The coupling spring between the two disks enables strong mechanical interaction between the two resonators. The scattering loss from the coupling beam is kept to a minimum by using a small beam

width of 0.5µm. To prevent mass loading and additional resonances, the coupling beam length needs to be half wavelength at the resonance. This however turns out to be too long, and a value of 1.5µm is chosen which is much less than the quarter wavelength at 288 MHz.

FABRICATION

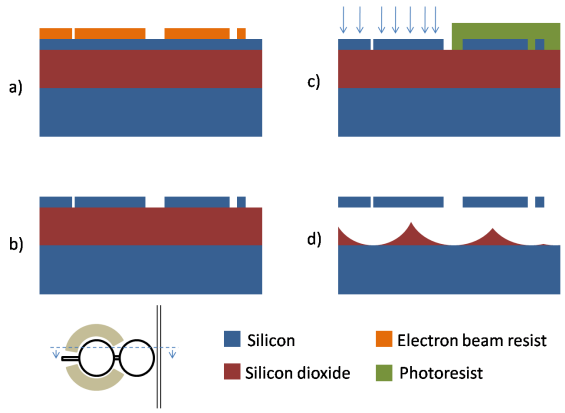

Figure 4. *Process flow for AOM fabrication: a) E-beam resist patterned b)Pattern transferred to silicon device layer by HBr ICP etch c) Ion implantation of the mechanical resonators, and d) Vapor HF etch*

The AOM is fabricated using a three mask process on a custom "photonic-SOI" wafer (undoped 250 nm device layer for low optical loss and 3µm thick buried oxide for isolation of the waveguides on device layer from the silicon substrate). Resist is spun on top of the silicon and patterned using electron beam lithography. The patterns are transferred into the silicon using an HBr based ICP RIE etcher to define the AOM, waveguides and bond-pads. A second resist mask is used to open implant windows to dope the MEMS resonators, electrodes and bond pads. We then pattern release windows near the modulator followed by a timed release etch in vapor HF to undercut the devices (Figure 4). An optical microscope image of an AOM is shown in figure 5.

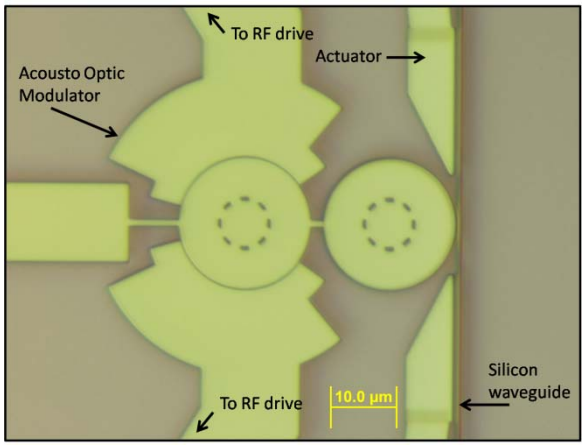

Figure 5. *Optical microscope image of the acousto-optic modulator. The actuators [11] are used to achieve critical coupling of the optical resonator and Si waveguide.*

EXPERIMENTAL SETUP

To test the performance of the mechanical resonators, a few devices with electrodes around both resonators are fabricated. These mechanical resonators are first tested using a two port mixing setup. A mechanical resonance frequency of 288 MHz and a quality factor of 11,890 in vacuum is obtained by the measurement which is as expected for the first radial mode of a 10µm radius disk resonator.

To measure the optical resonance characteristics, light from a tunable laser is coupled into the waveguide with the help of a cleaved fiber end and grating coupler. The light output from the device is recollected from an output grating into a cleaved fiber and sent to a photodiode. The transmission spectrum like that shown in figure 3 is obtained by sweeping the tunable laser and collecting the output of the photodiode. An optical Q of 6200 is obtained for resonance at 1560 nm and an extinction of 12 dB. The power input from the laser is 10 dBm and the output power level off optical resonance is -21 dBm.

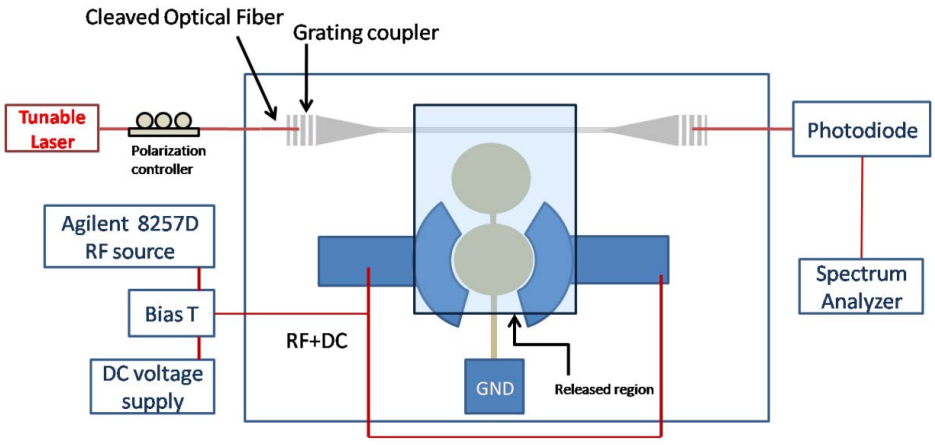

Figure 6. *Experimental setup for characterizing the silicon acousto-optic modulator*

The response of the acousto-optic modulator is observed with the setup shown in figure 6. The tunable laser is fixed at the 3 dB point of the optical resonance which is 1559.88 nm. A RF source is connected via a bias-T to the electrodes of the mechanical resonator. The photodiode is connected to a spectrum analyzer to look at the frequency content of the output light. The photodiode generates a current output proportional to the optical power input given by the responsivity of the detector. The responsivity of the photodiode is 1 A/W at 1560nm. The RF source is stepped and a spectrum analyzer measurement is obtained for each step to observe the response at the source frequency.

RESULTS

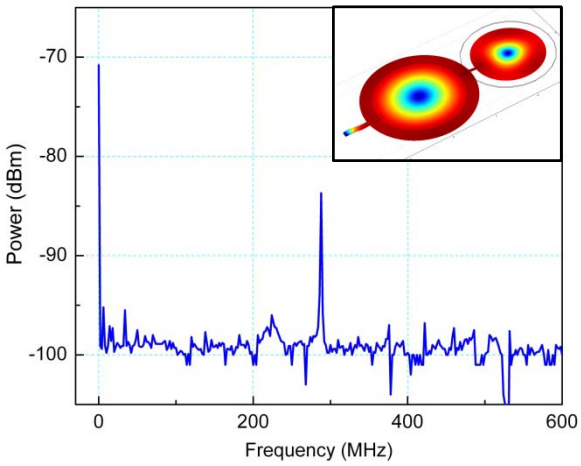

Figure 7. *Power spectrum at the output of the silicon acousto-optic modulator. The power at DC corresponds to the optical power transmitted through the modulator at the optical 3dB bias point. (inset) Mode shape obtained using COMSOL showing displacement for resonance at 288MHz*

The acousto-optic modulator is characterized in a Lakeshore FWP6 vacuum probe station which has been modified to accommodate optical i/o. We actuate the MEMS resonators by applying 10dBm RF power at 288 MHz along with a 15 V DC bias. The large input power is necessary to overcome the sheet resistance and inefficient transduction of the 103 nm air-gap transducer, and still get sufficient radial motion of both the MEMS and photonic resonators.

The power of -83.7dBm at the output at 288 MHz corresponds to current variation amplitude at the output of the photo-detector of 415 nA leading to an amplitude variation of ±415 nW around the optical bias of 3.98 µW at the output (Figure 7). The bandwidth of the modulator is given by the ratio of operating frequency to the mechanical quality factor of the resonator. For a quality factor of 11,890 in vacuum, the bandwidth of the modulator is 24.22 kHz.

CONCLUSION

We have demonstrated the first acousto-optic modulator in silicon. Recently, excellent progress has been demonstrated in exciting mechanical vibrations using radiation pressure [12] and optical gradient forces [13] in silicon to 2 GHz. The silicon acousto-optic modulator complements that work by demonstrating a monolithic narrow-bandwidth RF filter integrated with an up-converting radio→optical modulator at 288 MHz.

ACKNOWLEDGMENTS

The authors wish to thank Professor Farhan Rana, the Cornell Nanophotonics Group and ARL. This work was supported by the DARPA Young Faculty Award (Grant#: HR0011-08-1-0054).

REFERENCES

[1] A. Korpel, "Acousto-optics - A review of fundamentals," *Proc. of the IEEE* **69**(1) 48-53 (1981)

[2] C. Gorecki, et al., "Silicon-based integrated interferometer with phase modulation driven by surface acoustic waves," Optics Letters **22** 1784-86 (1997).

[3] P. Batista, et al, "ZnO/SiO_2 microcavity modulator on silicon," APL **92** 133502 (2008).

[4] N. Courjal, et al, "$LiNbO_3$ acousto-optical and electro-optical micromodulators", Journal of European Optical Society **4** 09018 (2009).

[5] X.Yao, L. Maleki, "Optoelectronic oscillators for photonic systems," J. of Quantum Electronics **32** (7) 1142-1149 (1996).

[6] C. Gunn, "A low phase noise 10GHz optoelectronic RF oscillator implemented using CMOS photonics," ISSCC 2007, pp. 570-571.

[7] L. Chen, M. Lipson, et al, "Integrated GHz silicon photonic interconnect with micrometer-scale modulators and detectors," Optics Express **17**(17) 15428 (2009).

[8] M. Soltani, "Novel Integrated Silicon Nanophotonic Structures using Ultra-high *Q* Resonators", Ph.D. Dissertation, GeorgiaTech, December 2009.

[9] Q. Xu, M. Lipson, et al,, "Micrometre-scale silicon electro-optic modulator," Nature **435**, 325-327 (2005).

[10] J. Clark, C. Nguyen, et al, "High-Q UHF micromechanical radial-contour mode disk resonators," JMEMS **14**(6) 1298-1310 (2005).

[11] M. Lee, Ming Wu, "Tunable coupling regimes of silicon microdisk resonators using MEMS actuators," Optics Express **14** 4703-4712 (2006).

[12] M. Eichenfield, O.Painter, et al, "Optomechanical crystals," Nature **462** 78-82 (2009).

[13] M. Li, et al, "Tunable bipolar optical interactions between guided lightwaves," Nature Photonics **3** 464-468 (2009).